

Collision geometry scaling of Au+Au pseudorapidity density from $\sqrt{s_{NN}}=19.6$ to 200 GeV

B. B. Back,¹ M. D. Baker,² M. Ballintijn,³ D. S. Barton,² R. R. Betts,⁴ A. A. Bickley,⁵ R. Bindel,⁵ A. Budzanowski,⁶ W. Busza,³ A. Carroll,² M. P. Decowski,³ E. García,⁴ N. George,^{1,2} K. Gulbrandsen,³ S. Gushue,² C. Halliwell,⁴ J. Hamblen,⁷ G. A. Heintzelman,² C. Henderson,³ D. J. Hofman,⁴ R. S. Hollis,⁴ R. Hołyński,⁶ B. Holzman,² A. Iordanova,⁴ E. Johnson,⁷ J. L. Kane,³ J. Katzy,^{3,4} N. Khan,⁷ W. Kucewicz,⁴ P. Kulinich,³ C. M. Kuo,⁸ W. T. Lin,⁸ S. Manly,⁷ D. McLeod,⁴ A. C. Mignerey,⁵ R. Nouicer,⁴ A. Olszewski,⁶ R. Pak,² I. C. Park,⁷ H. Pernegger,³ C. Reed,³ L. P. Remsberg,² M. Reuter,⁴ C. Roland,³ G. Roland,³ L. Rosenberg,³ J. Sagerer,⁴ P. Sarin,³ P. Sawicki,⁶ W. Skulski,⁷ P. Steinberg,² G. S. F. Stephens,³ A. Sukhanov,² M. B. Tonjes,⁵ J.-L. Tang,⁸ A. Trzupek,⁶ C. Vale,³ G. J. van Nieuwenhuizen,³ R. Verrier,³ F. L. H. Wolfs,⁷ B. Wosiek,⁶ K. Woźniak,⁶ A. H. Wuosmaa,¹ and B. Wyslouch³
(PHOBOS Collaboration)

¹Physics Division, Argonne National Laboratory, Argonne, Illinois 60439-4843, USA

²Chemistry and C-A Department, Brookhaven National Laboratory, Upton, New York 11973-5000, USA

³Laboratory for Nuclear Science, Massachusetts Institute of Technology, Cambridge, Massachusetts 02139-4307, USA

⁴Department of Physics, University of Illinois at Chicago, Chicago, Illinois 60607-7059, USA

⁵Department of Chemistry, University of Maryland, College Park, Maryland 20742, USA

⁶Institute of Nuclear Physics PAN, Kraków, Poland

⁷Department of Physics and Astronomy, University of Rochester, Rochester, New York 14627, USA

⁸Department of Physics, National Central University, Chung-Li, Taiwan

(Received 25 May 2004; published 24 August 2004)

The centrality dependence of the midrapidity charged particle multiplicity in Au+Au heavy-ion collisions at $\sqrt{s_{NN}}=19.6$ and 200 GeV is presented. Within a simple model, the fraction of hard (scaling with number of binary collisions) to soft (scaling with number of participant pairs) interactions is consistent with a value of $x=0.13\pm0.01(\text{stat})\pm0.05(\text{syst})$ at both energies. The experimental results at both energies, scaled by inelastic $p(\bar{p})+p$ collision data, agree within systematic errors. The ratio of the data was found not to depend on centrality over the studied range and yields a simple linear scale factor of $R_{200/19.6}=2.03\pm0.02(\text{stat})\pm0.05(\text{syst})$.

DOI: 10.1103/PhysRevC.70.021902

PACS number(s): 25.75.Nq, 25.75.Dw

We have studied the centrality dependence of the charged particle multiplicity at midrapidity for Au+Au collisions at nucleon-nucleon center of mass energies $\sqrt{s_{NN}}=19.6$ and 200 GeV, using the PHOBOS detector at the Relativistic Heavy Ion Collider (RHIC) in Brookhaven National Laboratory. Data at both energies have allowed the extraction of results with the same detector, which covers a factor of 10 in collision energy, from slightly above the highest energy of the CERN SPS fixed target program to the highest RHIC energy.

Recent results from RHIC have suggested the effect of “jet quenching” in central Au+Au collisions that acts to reduce both the overall yield of high p_T particles [1–3] and back-to-back jet correlations [4]. The presence of these dramatic effects for the most central Au+Au collisions at $\sqrt{s_{NN}}=130$ and 200 GeV, as well as their absence in the cases of peripheral Au+Au [1–3], central d +Au [5,6] and inclusive d +Au [7,8] have been generally well reproduced by calculations that utilize a p QCD framework to calculate the initial high p_T production rates, coupled with a large energy loss in the dense medium [9]. In this picture, the produced “dense medium” is responsible for the experimental effect, which presumably occurs only in the large overlap volume of central Au+Au collisions.

One of the intriguing overall features of the RHIC data, however, is that models solely based on parton saturation in the colliding nuclei describe the detailed centrality and rapid-

ity dependence of the measured charged particle multiplicities at 130 and 200 GeV [10,11]. If parton saturation is playing a significant role in these relativistic heavy ion collisions, it could also reduce the initial production rate of high p_T particles to the extent that a large energy loss in the dense medium is no longer necessary to describe the data for central Au+Au collisions [2,11]. Since the measured total charged particle multiplicities are completely dominated by the emission of low p_T (≤ 1.5 GeV/ c) particles, one might speculate that the production dynamics of low p_T particles is quite different from those at high p_T . A study of the detailed centrality dependence of the bulk charged particle production over a large energy range may, therefore, provide additional constraints on models attempting to describe both the low and high p_T behavior of particle production.

The PHOBOS detector configuration was the same for measurements at $\sqrt{s_{NN}}=19.6$ and 200 GeV. Specifically, the detectors used in this analysis were the centrally located Octagon barrel, Vertex detector and the multiplane Spectrometer. These detectors are all constructed from silicon wafers, more details can be found in Refs. [12,13]. The primary trigger for the data reported here is based on $n > 2$ hits in two segmented, large-area scintillator counter arrays (Paddles) covering $3.2 < |\eta| < 4.5$ relative to the nominal vertex position. Pseudorapidity is defined as $\eta = -\ln \tan(\theta/2)$ where θ is the polar angle to the beam axis. This trigger was sensitive to 88% of the total inelastic cross section in the 200 GeV data

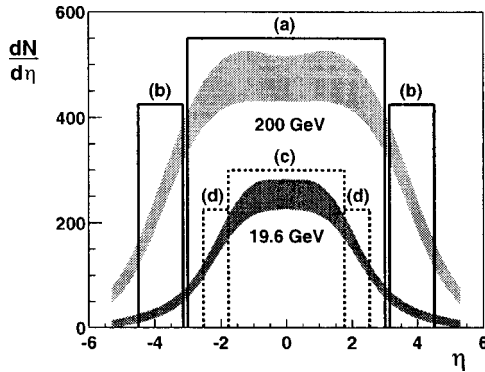


FIG. 1. Pseudorapidity density distributions from $\sqrt{s_{NN}}=200$ (light band) and 19.6 (dark band) GeV Au+Au collisions, for the most central 25% of the cross section [17]. The boxed areas (a)–(d) illustrate the separate regions in pseudorapidity used for the centrality determinations at each energy.

[12] and is estimated to be 80% efficient for 19.6 GeV, from Monte Carlo (MC) studies using Hijing [14] and a full GEANT [15] simulation of the PHOBOS detector.

The centrality determination for the PHOBOS Au+Au results at $\sqrt{s_{NN}}=130$ and 200 GeV [10,16] uses the energy signals from the Paddle counters, which lie away from midrapidity, as illustrated by region (b) in Fig. 1. These signals, through bins in the percentage of total cross section, provide a measure of centrality. A similar centrality measure can be created at 19.6 GeV by scaling the Paddle pseudorapidity range by the ratio of beam rapidities at 200 and 19.6 GeV, $y_{19.6}^{Beam}/y_{200}^{Beam}=0.563$, as shown in region (d) of Fig. 1. The resulting η region, $1.8 < |\eta| < 2.5$, lies within the Octagon detector coverage of $|\eta| \leq 3.2$ for collisions within ± 10 cm of the nominal vertex position. Thus, a centrality measure based on the deposited energy in this specific region (d) of the Octagon was calculated for 19.6 GeV and used in determining centrality for direct comparison to the original Paddle based centrality determination at 200 GeV.

A second, independent, centrality measure was also developed for both data sets. This was based on the energy of charged particles traversing the Octagon within $|\eta| < 3.0$ at 200 GeV, region (a) of Fig. 1, and a “reduced” region of $|\eta| < 1.8$ at 19.6 GeV, region (c).

The vertex position of each event is required for the merging and angle correction of valid hits in the Octagon. The primary collision vertex used was determined by straight-line tracks in the first six planes of the Spectrometer. The same vertexing algorithm was used at both energies. From MC studies of the detector, this vertex has a resolution $\sigma_{x,y,z} \approx 0.3, 0.3, 0.4$ mm for central and $\sigma_{x,y,z} \approx 0.6, 0.5, 0.8$ mm for mid-peripheral collisions at 19.6 GeV, where z is along the beam and y is vertical. For more peripheral collisions, the efficiency falls away smoothly from 100% with decreasing centrality. Additional cross-checks performed with different vertexing methods yielded consistent results.

Due to the requirement of a valid vertex, the resulting data set is not only biased by the intrinsic trigger efficiency, but also by our (track-based) vertex reconstruction efficiency. The vertex biased detection efficiency at 200 GeV is deduced from prior measurement [12]. At 19.6 GeV, the effi-

ciency is determined from a ratio of yields (Data/MC) after shape matching of multiplicity distributions between data and MC simulations in the centrality regions (c) or (d) from Fig. 1. The matching algorithm only utilizes data where 100% efficiency in both triggering and vertexing is expected. The overall efficiency, including the trigger and vertexing bias, is estimated to be $66.0 \pm 2.0\%$ and $55.4 \pm 2.0\%$ for the 200 and 19.6 GeV data, respectively.

The final step in the centrality determination is to connect the experimentally deduced cross section percentiles with a well-defined variable, such as the number of participating nucleons, N_{part} . In order to do this, a monotonic relation was assumed to exist between the multiplicity distribution in the chosen η region and N_{part} . This assumption has been borne out by extensive simulations and the experimental (inverse) correlation between multiplicity and zero degree calorimetry. Additionally, in order to further reduce ambiguity in this assumption, the measures of centrality outlined above were chosen specifically to lie in very different regions of pseudorapidity. Away from midrapidity, regions (b) and (d), particle production in the Hijing model depends linearly on N_{part} , as discussed in Ref. [18]. However, the midrapidity charged particle production, regions (a) and (c), is not linear as predicted by Hijing. Comparison of the results from these distinct regions for centrality determination can expose any systematic effects of non-linearity.

The “tracklet” reconstruction method was used to obtain the best measure of the charged particle multiplicity at midrapidity. A tracklet is a two-hit combination from the inner and outer Vertex detector layers, which points back to the reconstructed vertex. A tracklet is only formed when the difference between the hits (residuals) in azimuthal angle and η are less than 0.3 rad and 0.04, respectively. The difference in the magnitude of these values originates from the granularity of the detector in the respective measured directions. The final multiplicity is measured in the region $|\eta| < 1$ by counting all reconstructed tracklets and correcting for detector acceptance (acc), combinatorial background (comb) and additional background from secondary particles and weak decays (s+w). For a nominal vertex position ($z=0$) these multiplicative factors are approximately 3.57 (acc), 0.74 (comb) and 0.97 (s+w). The resulting correction factor, determined using MC simulations as a function of reconstructed vertex position and number of hits in the vertex detector, is found to be the same for each energy to within 1%. Results obtained using centrality regions (a) and (c) of Fig. 1 are given in Table I. We obtain the same result for the yield per participant pair, $dN_{ch}/d\eta/(\frac{1}{2}\langle N_{part} \rangle)$, from centrality regions (b) and (d). Systematic errors for the Vertex detector tracklet results, as in [10], are 7.5% (90% C.L.) at both energies.

An independent analysis was also carried out at both energies using tracklets from pairs of hits in adjacent Spectrometer planes. This additional analysis yielded results consistent, within 2%, with the presented data.

The data for 19.6 GeV, together with the reanalyzed results for 200 GeV, are shown in Fig. 2. This new result for 200 GeV has a slightly flatter dependence on $\langle N_{part} \rangle$ than found previously [10], but within the quoted systematic er-

TABLE I. Experimental results for the charged particle pseudorapidity density at midrapidity as a function of percentile cross section. The most central collisions are labeled as Bin 0–3%. The requirement of 100% efficiency in both triggering and vertexing imposes a lower limit on the reported results of $\langle N_{part} \rangle \geq 65$ and 95 for 200 and 19.6 GeV, respectively. All errors represent 90% C.L. systematic limits with the exception of the Ratio, for which the errors are standard combined statistical and systematic 1- σ uncertainties.

Bin(%)	200 GeV			19.6 GeV			Ratios
	$dN_{ch}/d\eta$	$\langle N_{part} \rangle$	$dN_{ch}/d\eta / (\frac{1}{2}\langle N_{part} \rangle)$	$dN_{ch}/d\eta$	$\langle N_{part} \rangle$	$dN_{ch}/d\eta / (\frac{1}{2}\langle N_{part} \rangle)$	
0–3	691±52	361±11	3.82±0.31	331±24	351±11	1.89±0.15	2.03±0.06
3–6	619±46	331±10	3.74±0.30	297±22	322±10	1.84±0.15	2.03±0.06
6–10	540±41	297±9	3.64±0.30	260±20	286±9	1.82±0.15	2.00±0.06
10–15	465±35	255±8	3.65±0.30	216±16	247±8	1.76±0.14	2.08±0.07
15–20	384±29	215±7	3.57±0.29	181±14	206±8	1.75±0.15	2.04±0.08
20–25	313±24	180±7	3.47±0.30	148±11	171±7	1.73±0.15	2.01±0.09
25–30	257±19	150±6	3.42±0.29	121±9	142±7	1.70±0.15	2.01±0.12
30–35	208±16	124±6	3.37±0.30	97±7	117±7	1.65±0.16	2.03±0.13
35–40	165±12	101±6	3.25±0.31	78±6	95±7	1.64±0.17	1.98±0.14
40–45	133±10	82±6	3.25±0.34				
45–50	100±8	65±6	3.10±0.38				

rors. This flattening of the yield with $\langle N_{part} \rangle$ for central collisions arises entirely from the new (vertex restricted) centrality measures and methods detailed above. This result also agrees within errors with published data from other RHIC experiments at 200 GeV [19–21], although the trends of the centrality dependence differ. For 19.6 GeV, we find reasonable agreement with results from NA49 [22] and NA50 [23] for central Pb+Pb collisions at the highest SPS energy ($\sqrt{s_{NN}}=17.2$ GeV), after correction for the known frame and energy dependence. Results from EMU-13 at the SPS appear to be $\approx 15\%$ lower [24], and experiment WA98 published a

detailed centrality dependence [25] that is similar to this measurement, however their overall charged particle multiplicity is $\approx 20\%$ higher.

The inelastic charged particle multiplicity obtained in $p(\bar{p})+p$ collisions [26,27] is given in Fig. 2 at $N_{part}=2$ for data measured at 200 GeV ($dN_{ch}/d\eta|_{|\eta|<1}=2.29\pm 0.08$) and interpolated for 19.6 GeV ($dN_{ch}/d\eta|_{|\eta|<1}=1.27\pm 0.13$). The $p(\bar{p})+p$ data are averaged over the same pseudorapidity, $|\eta|<1$, as the heavy ion measurement. Clearly, the yield of charged particles per participant pair for the measured Au+Au collisions is higher than found in corresponding $p(\bar{p})+p$ collisions.

The dotted line in Fig. 2 represents a fit to the data using the simple two-component parameterization proposed in Ref. [28]:

$$\frac{dN_{ch}}{d\eta} = n_{pp} \left((1-x) \frac{\langle N_{part} \rangle}{2} + x \langle N_{coll} \rangle \right).$$

The value for N_{coll} , the number of binary (nucleon-nucleon) collisions, is determined from a Glauber model calculation and is found to depend on the number of participants, N_{part} , through a simple power law. We find that $N_{coll}=A \times N_{part}^\alpha$ with $A=0.33$ and 0.37 and $\alpha=1.37$ and 1.32 for 200 and 19.6 GeV, respectively. The difference in the A and α parameters at the two energies is due to the measured nucleon-nucleon cross sections at $\sqrt{s_{NN}}=200$ GeV ($\sigma_{NN}=42\pm 1$ mb) vs. 19.6 GeV ($\sigma_{NN}=33\pm 1$ mb). The remaining parameters are n_{pp} , the yield obtained in $p(\bar{p})+p$ collisions, and x , which represents the contribution from “hard” processes taken to scale with N_{coll} .

The large systematic errors on the data preclude a simultaneous extraction of both n_{pp} and x solely from the Au+Au data. If only statistical errors are considered, the ex-

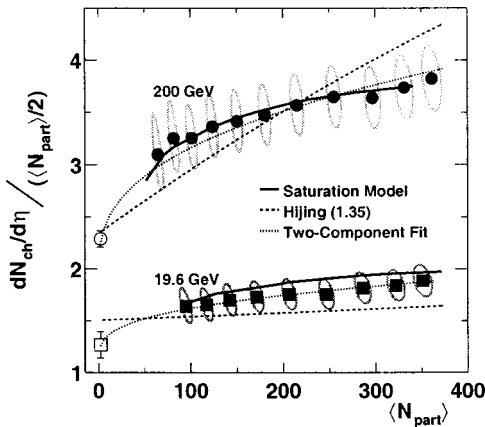


FIG. 2. The measured midrapidity ($|\eta|<1$) pseudorapidity density per participant pair as a function of $\langle N_{part} \rangle$ for Au+Au collisions at $\sqrt{s_{NN}}=19.6$ GeV (closed squares), 200 GeV (closed circles). Error ellipses around the data combine the systematic error on $dN_{ch}/d\eta|_{|\eta|<1}$ and $\langle N_{part} \rangle$. The open symbols represent the $p(\bar{p})+p$ results (see the text). The three curves give two model calculations and one fit result. As in [10], the systematic errors represent 90% C.L. limits.

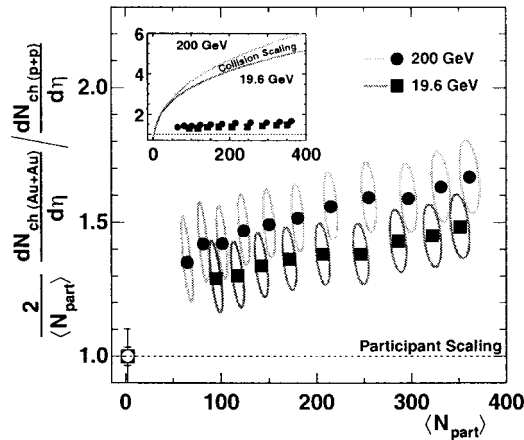


FIG. 3. Centrality dependence of the measured Au+Au pseudorapidity density per participant pair divided by the corresponding value obtained in $p(\bar{p})+p$ collisions. There is an additional scale error associated with the error on the value of the $p(\bar{p})+p$ data points of 3.5% and 10% for the 200 and 19.6 GeV data, respectively. The inset has the same axes labels as the main figure, with curved lines representing the binary collision (N_{coll}) scaling limit for both energies and the horizontal dashed line corresponding to pure N_{part} scaling. As in Fig. 2, error ellipses represent 90% C.L. limits.

tracted parameters are $n_{pp} \approx 2.7$, 1.3 and $x \approx 0.09$, 0.11 at 200 and 19.6 GeV, respectively.

A value for x can also be obtained by fixing n_{pp} at the measured and interpolated values of 2.29 and 1.27. Using statistical errors, we find $x=0.145$ and 0.120 for 200 and 19.6 GeV, respectively, as depicted by the dotted line in Fig. 2. The systematic error on the fit parameter x was determined by allowing the pp value and the data points to vary independently within their systematic uncertainties. Within the systematics, we find that the fraction of hard collisions for both energies is consistent with a single value of $x = 0.13 \pm 0.01(\text{stat}) \pm 0.05(\text{syst})$.

The equivalence of parameter x at both energies, within the large errors, is surprising as the p QCD cross section for processes with large momentum transfers is expected to rise from $\sqrt{s_{NN}}=19.6$ to 200 GeV. This expectation of increasing slope in centrality with collision energy is shown by the dashed lines in Fig. 2, which represent Hijing predictions [14]. Although this rapid rise is not conclusively ruled out within the systematics at $\sqrt{s_{NN}}=200$ GeV, it clearly does not follow the trend found in the data. Calculations from the parton saturation model [11,29] (solid lines in Fig. 2) predict a much weaker centrality dependence for both energies, in better agreement with the experimental data.

In order to gain a different perspective on the data, we scale the Au+Au charged particle pseudorapidity density at midrapidity by that obtained in inelastic $p(\bar{p})+p$ collisions at the same collision energy, shown in Fig. 3. The similarity between the two data sets is remarkable. The inset in Fig. 3 shows the data with an expanded y -range and additional curved lines illustrating the expectation for pure binary collision (N_{coll}) scaling at 200 and 19.6 GeV. The dashed horizontal line represents the expectation for pure participant (N_{part}) scaling. In this representation, it becomes clear that

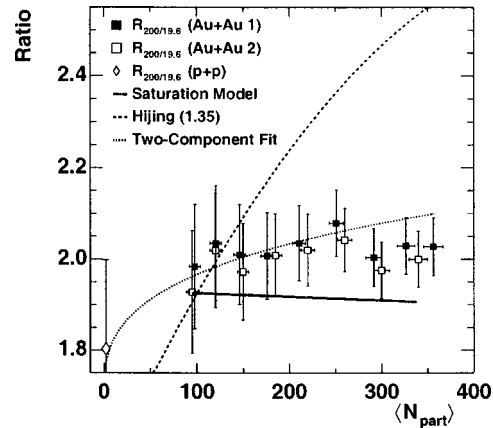


FIG. 4. The ratio, $R_{200/19.6}$, of the midrapidity pseudorapidity density per participant pair at 200 and 19.6 GeV versus $\langle N_{part} \rangle$, binned by fraction of cross section (closed squares) and by matching $\langle N_{part} \rangle$ (open squares). The ratio of inelastic $p(\bar{p})+p$ collision data is given at $N_{part}=2$ (open diamond). Curves give various calculations. The vertical error bars are combined statistical and systematic $1-\sigma$ uncertainties.

the data at both energies follow a more N_{part} -like dependence.

Systematic errors dominate the charged particle density measurements at 200 and 19.6 GeV. We find, however, that most of these cancel in the ratio, leaving a baseline 3.0% overall uncertainty. This occurs as both analyses were performed with exactly the same method, detector and with carefully matched centrality determinations. The main uncertainty comes from statistics of data and MC simulations (2.2%) and systematics in the primary charged particle detection efficiency (2.0%). Smaller systematic contributions arise from background subtraction (0.4%) and uncertainty in the nucleon-nucleon cross section, σ_{NN} (0.4%). We also include an additional centrality dependent systematic uncertainty that is largest in the more peripheral region and becomes negligible for the most central. This term takes into account the possibility that the estimated overall efficiency error may not entirely cancel in the ratio.

As a final cross-check, the ratio of data at 200 to 19.6 GeV, $R_{200/19.6}$ is calculated in two distinct ways. First, a more model-independent ratio was formed by dividing the data at each corresponding fraction of total interaction cross section. This is given by the closed squares in Fig. 4 (Au+Au 1). Matching the centrality percentile bin at each energy, however, means there will be a difference in the deduced $\langle N_{part} \rangle$ value at 19.6 and 200 GeV (see Table I). In this case, the assigned $\langle N_{part} \rangle$ for each percentile bin given in the figure is taken as the average of the two individual $\langle N_{part} \rangle$ values. Second, the ratio was formed using a new set of centrality cuts for which each centrality bin width was varied, in an iterative fashion, in order to obtain bins at both 19.6 and 200 GeV that yield the same calculated average N_{part} . The data at both energies were then completely re-analyzed using this second set of centrality cuts. This result is given by the open squares of Fig. 4 (Au+Au 2).

The results from the two types of ratio calculations are shown in Fig. 4, together with the predictions of two models

and the two-component fit from Fig. 2. We find that both sets of data (closed and open squares) are in agreement, even within the significantly reduced systematic errors. Additionally, we find that the slope, and hence the centrality dependence, of both ratios is zero, within error. The most probable mean value of the (Au+Au 1) ratio data is found to be $R_{200/19.6} = 2.03 \pm 0.02(\text{stat}) \pm 0.05(\text{syst})$. We remind the reader that the ratio of 200 to 130 GeV data was found to be $R_{200/130} = 1.14 \pm 0.01(\text{stat}) \pm 0.05(\text{syst})$ [10].

With the reduced systematic errors on the ratio now available, we return to a more detailed comparison of our results to calculations. As shown in Fig. 4, model calculations predict quite different centrality dependencies of $R_{200/19.6}$ over the collision energy range of 19.6 to 200 GeV. We find that the Hijing calculation gives the expected increase from p QCD minijet production with centrality over this energy range, but the predicted increase is now in strong contradiction to the data. The flat centrality dependence of the ratio is relatively well described by the parton saturation model calculation.

In summary, PHOBOS has measured the charged particle

pseudorapidity density at midrapidity ($|\eta| < 1$) for Au+Au collisions at energies of $\sqrt{s_{NN}} = 19.6$ and 200 GeV. We find an increase in particle production per participant pair for Au + Au collisions compared to inelastic $p(\bar{p}) + p$ values for both energies. The ratio of the measured yields at 200 and 19.6 GeV shows a clear geometry scaling over the central 40% inelastic cross section and averages to $R_{200/19.6} = 2.03 \pm 0.02(\text{stat}) \pm 0.05(\text{syst})$. A large increase in yield from hard processes, which contribute to multiplicity, is not apparent in the data, even over an order of magnitude range of collision energy.

We express appreciation to the BNL management for approving the one day of 19.6 GeV running. This work was partially supported by U.S. DOE grants DE-AC02-98CH10886, DE-FG02-93ER40802, DE-FC02-94ER40818, DE-FG02-94ER40865, DE-FG02-99ER41099, and W-31-109-ENG-38, US NSF grants 9603486, 9722606 and 0072204, Polish KBN grant 2-P03B-10323, and NSC of Taiwan contract NSC 89-2112-M-008-024.

-
- [1] K. Adcox *et al.*, Phys. Rev. Lett. **88**, 022301 (2002).
 - [2] J. Adams *et al.*, Phys. Rev. Lett. **91**, 172302 (2003).
 - [3] B. B. Back *et al.*, Phys. Lett. B **578**, 297 (2004).
 - [4] C. Adler *et al.*, Phys. Rev. Lett. **90**, 082302 (2003).
 - [5] B. B. Back *et al.*, Phys. Rev. Lett. **91**, 072302 (2003).
 - [6] J. Adams *et al.*, Phys. Rev. Lett. **91**, 072304 (2003).
 - [7] I. Arsene *et al.*, Phys. Rev. Lett. **91**, 072305 (2003).
 - [8] S. S. Adler *et al.*, Phys. Rev. Lett. **91**, 072303 (2003).
 - [9] M. Gyulassy *et al.*, nucl-th/0302077.
 - [10] B. B. Back *et al.*, Phys. Rev. C **65**, 061901(R) (2002).
 - [11] D. Kharzeev and E. Levin, Phys. Lett. B **523**, 79 (2001).
 - [12] B. B. Back *et al.*, Phys. Rev. Lett. **88**, 022302 (2002).
 - [13] B. B. Back *et al.*, Nucl. Instrum. Methods Phys. Res. A **499**, 603 (2003).
 - [14] M. Gyulassy and X. N. Wang, Comput. Phys. Commun. **83**, 307 (1994). Version 1.35 is used.
 - [15] GEANT 3.21, CERN Program Library, Geneva.
 - [16] B. B. Back *et al.*, Phys. Rev. C **65**, 031901(R) (2002).
 - [17] B. B. Back *et al.*, Phys. Rev. Lett. **91**, 052303 (2003).
 - [18] X. N. Wang and M. Gyulassy, Phys. Rev. Lett. **86**, 3496 (2001).
 - [19] I. G. Bearden *et al.*, Phys. Rev. Lett. **88**, 202301 (2002).
 - [20] A. Bazilevsky, Nucl. Phys. **A715**, 486c (2003).
 - [21] J. Adams *et al.*, Phys. Rev. Lett. **92**, 112301 (2004).
 - [22] H. Appelhauser *et al.*, Phys. Rev. Lett. **82**, 2471 (1999); S. F. Afanasiev *et al.*, Phys. Rev. C **66**, 054902 (2002).
 - [23] M. C. Abreu *et al.*, Phys. Lett. B **530**, 33 (2002); **530**, 43 (2002).
 - [24] P. Deines-Jones *et al.*, Phys. Rev. C **62**, 014903 (2000).
 - [25] M. M. Aggarwal *et al.*, Eur. Phys. J. C **18**, 651 (2001).
 - [26] G. J. Alner *et al.*, Z. Phys. C **33**, 1 (1986); R. E. Ansorge *et al.*, *ibid.* **43**, 357 (1989).
 - [27] W. Thomé *et al.*, Nucl. Phys. **B129**, 365 (1977).
 - [28] D. Kharzeev and M. Nardi, Phys. Lett. B **507**, 121 (2001).
 - [29] D. Kharzeev, E. Levin, and M. Nardi, hep-ph/0111315.